metals

MDPI

Article

Material Behavior of High-Strength Low-Alloy Steel (HSLA) WAAM Walls in Construction

Hendrik Jahns [1,*,†], Julian Unglaub [1,†], Johanna Müller [2], Jonas Hensel [2] and Klaus Thiele [1]

[1] Institute of Steel Structures, Technische Universität Braunschweig, 38106 Braunschweig, Germany
[2] Welding Engineering, Institute of Joining and Assembly, Chemnitz University of Technology, 09126 Chemnitz, Germany
* Correspondence: h.jahns@stahlbau.tu-braunschweig.de
† These authors contributed equally to this work.

Abstract: Additive manufacturing with steel offers new opportunities for the construction sector. In particular, direct energy deposition (DED) processes such as Wire Arc Additive Manufacturing (WAAM or DED-Arc), are able to create large structures with a high degree of geometric freedom, like force-flow-optimized steel nodes and frameworks, as well as truss structures. By using high-strength steel, manufacturing times can be shortened because less material has to be applied. In order to enable the usage of WAAM components in the construction industry, profound knowledge of the material behavior is necessary. Based on reliable process parameters, extensive experimental and numerical investigations are carried out to characterize the influence of layer orientation and overhang angle on the mechanical parameters of WAAM high-strength low-alloy steel (HSLA) walls. The results have been compared to HSLA steel sheet material. It is shown that comparable characteristics exist for Young's modulus E, yield strength $R_{p,0.2}$ and tensile strength R_m with regard to civil engineering applications. The influence of the loading direction on the material level is similar. Only the yield strength shows a slight dependence on the layer orientation for WAAM walls (difference 4.5%). The overhang angle has no influence on the material parameters.

Keywords: WAAM; DED-arc; HSLA; mechanical properties; material anisotropy; tensile coupon tests

check for updates

Citation: Jahns, H.; Unglaub, J.; Müller, J.; Hensel, J; Thiele, K. Material Behavior of High-Strength Low-Alloy Steel (HSLA) WAAM Walls in Construction. *Metals* **2023**, *13*, 589. https://doi.org/10.3390/met13030589

Academic Editor: Tomoyoshi Maeno

Received: 1 February 2023
Revised: 7 March 2023
Accepted: 9 March 2023
Published: 14 March 2023

Copyright: © 2023 by the authors. Licensee MDPI, Basel, Switzerland. This article is an open access article distributed under the terms and conditions of the Creative Commons Attribution (CC BY) license (https://creativecommons.org/licenses/by/4.0/).

1. Introduction

In the construction industry, it is common to use standardized semi-finished products such as I-beams or hollow sections fabricated by conventional methods. Joints between semi-finished parts require additional sheet material for local force transfer due to high stress concentrations. Especially in the direct joint area of hollow sections, cast components are used in addition to welded connections [1]. Although cast components permit a node design that is suitable for force flow, they can only be used economically, if a large number of identical nodes has to be manufactured. In addition, there are technological limits to the casting itself, e.g., varying wall thicknesses.

In architecture and civil engineering, the importance of individual constructions, combination of materials, lightweight structures and sustainability in the use of resources is growing. Additive manufacturing (AM) in construction offers the opportunity of free architectural design of steel components, e.g., thin shells and complex force flow optimized steel nodes.

Multiple technologies exist for the production of AM components. They are referred to as direct energy deposition (DED) processes and can be categorized by energy source: DED laser, DED-EB, and DED arc, commonly known as Wire Arc Additive Manufacturing (WAAM). WAAM processes use conventional welding processes such as GMAW, GTAW, or GPAW. These processes can be combined with a robotic system. This leads to a high degree of geometric freedom and is therefore suitable for the production of complex components. Advantages of the WAAM process are the high build-up rate and the variety of materials,

since they use conventional welding wires. Therefore, various alloys of steel, aluminum and titanium are generally usable.

One of WAAM's best-known applications in structural engineering is the MX3D stainless steel bridge in Amsterdam [2]. Another example of WAAM components are nodal connectors in lightweight structures [3–6]. The applicability of WAAM to large-scale structures, such as rocket fuel tanks, similar to silo structures in civil engineering, is demonstrated by RELATIVITYSPACE [7]. These examples show that WAAM is important in the construction industry. However, these are tailored applications with their own processes and their certifications are usually not in compliance with the design codes of the construction industry.

Previous studies with respect to structural application of material behavior of WAAM mainly focused on stainless steels [8–10] and mild steels [8,11,12]. Only a few studies have performed research on high-strength steel [12–15]. Moderate mechanical anisotropy was observed in both WAAM normal- and high-strength steels by [16,17], almost isotropic behavior was found by [8,12,15,18].

Ref. [10] analyzed data from tensile tests on machined specimens extracted from WAAM stainless steel sheets in order to investigate possible anisotropy. Different tensile test specimens have been cut out (0°, 45°, 90°) relative to the deposition direction. The tests show distinctly anisotropic material behavior. [9] performed tensile tests on WAAM stainless steel on milled specimens, in order to to quantify material anisotropy. The results showed that the layer orientation has a strong influence on the material behavior. Diagonal specimens have the highest Young's modulus and tensile strength, while vertical specimens have the lowest mechanical properties.

Ref. [11] carried out tensile tests on WAAM mild steel milled plates. The specimens were cut out in different directions (0°, 45°, 90°) with respect to the printing orientation to investigate possible material anisotropy. Their investigation shows that the influence of the printing direction on the Young's modulus, yield strength and tensile strength is negligible for structural applications. Only the elongation at break is slightly influenced by the printing direction.

Ref. [19] utilizes the WAAM process for the production of high-strength structural steel parts. From WAAM walls made of HSLA steel, specimens have been extracted in different directions (0°, 90°) with respect to the printing orientation to investigate possible material anisotropy. The tensile and yield strength did not change significantly with build-up direction, but the elongation at break exhibits up to 10% difference, indicating anisotropy for this parameter.

Ref. [12] undertook comprehensive experimental studies into the mechanical properties and the microstructure of WAAM plates made of mild and high-strength steels. Specimens have been cut out in different directions (0°, 30 °, 45°, 60 ° 90°). The specimens exhibited almost isotropic mechanical properties. For HSLA steel walls, only one build-up direction has been investigated. No overhangs were taken into account. Furthermore, their wall thickness of 3 mm is not representative for construction applications.

Ref. [20] explores the use of Submerged Arc Additive Manufacturing (SAAM) for manufacturing HSLA steel T-branch pipes. The material parameters in the horizontal and vertical direction of deposit (0°, 90° were studied on cut-out specimens. The horizontal and vertical tensile strengths were similar, but elongation at break of the the vertical specimens was lower than that of the horizontal ones.

Ref. [14] investigates the influences of welding energy input, interpass temperature, and cooling rate for welding thin-walled samples of high-strength steel. Tensile test specimen have been cut out in two directions (0°, 90°) in relation to the printing orientation. The diagonal direction has not been investigated. Their experiments show that the influence of printing direction on yield strength and tensile strength is negligible for practical construction applications. Only the elongation at break is influenced by the printing direction.

Ref. [9] used an isotropic two stage RAMBERG-OSGOOD model. To account for anisotropy, the anisotropy coefficients for every direction (0°, 45°, 90°) were averaged. A

first validation for a WAAM component has been performed in [21]. Investigations on the same data set by [10] showed that the anisotropy has to be taken into account. Therefore, Refs. [2,10] used an orthotropic plane stress material model for stainless steel with the definition of two Young's modulo. In the inelastic range, the anisotropy is described through the HILL yield criterion. This model was used to predict the global displacement of the MX3D bridge in the elastic regime. The comparisons of experimental and numerical data showed good agreement.

The focus of research has been mainly on the characterization of the material behavior of stainless steel and low-strength structural steel. Using HSLA steel in the construction industry can help reduce manufacturing time for large parts. Additionally, the use of high-strength steel reduces the amount of material required, which further contributes to the efficiency of the manufacturing process. The material behavior of HSLA steel with yield strengths of up to 800 MPa has not yet been comprehensively studied with regard to construction applications. The build-up direction is usually perpendicular to the substrate, overhangs have not yet been investigated. Especially on the material level, questions about the possible anisotropic behavior are still unresolved. Likewise, no adequate comparison of anisotropic/isotropic behavior between plate steel and WAAM has been carried out yet.

For a reliable application in civil engineering, there are still uncertainties regarding the material behavior of WAAM with HSLA steels and its modeling, despite the significant progress made in recent years in terms of process stability and manufacturing strategies. Therefore, this work carries out extensive experimental and numerical investigations to characterize the influence of layer orientation and overhang angle on the mechanical parameters of WAAM HSLA steel walls and compares the results to HSLA steel sheet material. For numerical investigations of WAAM components, an advanced material model is proposed and calibrated.

2. Materials and Methods

The process parameters have a significant influence on the material properties. An extensive process qualification was carried out by [14]. Based on these investigations, a suitable welding process set was selected for this study. Therefore, only the influence of different overhang angles on the material behavior was examined. In this section, the individual steps of the test routine and analysis will be explained step by step.

2.1. Specimen Manufacturing

The steel wire used is the low-alloyed, high-strength structural steel wire Böhler 3Dprint AM 80 HD, which has a diameter of 1.2 mm.

The 6-axis KUKA KR22 handling robot with a tilt-turn table manufactured the walls for the specimens using a Fronius TPS500i power source with the CMT Dynamic mode. The walls were deposited with an approximate layer height of 1.9 mm. To maintain the interpass temperature between layers, an infrared pyrometer type Dias Pyrospot DGE 44N mounted on the robot was used to measure the temperature in the middle of the last layer deposited. The interpass temperature was kept at 200 °C and an active cooling with compressed air with a flow rate of 12 m/s was used. The travel speed was kept constant at 25 cm/min. The process parameters were set to 2 m/min wire feed rate, 13.1 V welding voltage, 75 A welding current, which results in an energy input of 2.3 kJ/cm.

Three walls were manufactured with the previous welding parameters, two without an overhang angle and one with an overhang angle of 75°. The overhang angle is defined as the angle between the vertical axis and the build direction axis of the wall, therefore a 0° wall is a vertical wall (see Figure 1).

The specimens were cut out of the wall with a water jet. Horizontal alignment is defined as in the deposition direction, vertical as in the build direction and diagonal subsequently with an angle of 45°to both (see Figure 1). Afterwards, the specimen surface was machined to achieve a thickness of 3.5 mm. The specimen dimensions are given in Figure 2.

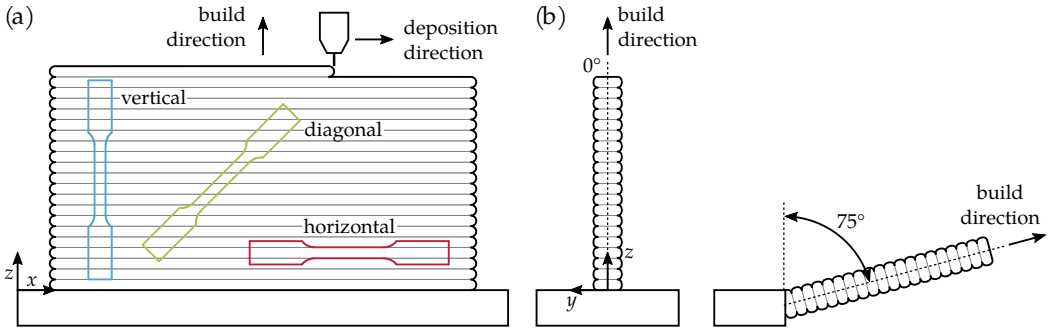

Figure 1. Specimen alignment in relation to build and deposition direction (**a**) and the overhang angle in relation to the vertical axis and the build direction (**b**).

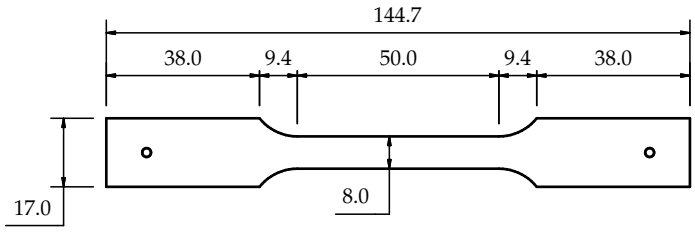

Figure 2. Cut-out tensile specimen dimensions in mm.

25 specimens were extracted from the walls, Table 1 lists the number of specimens per orientation and overhang angle.

Table 1. Number of specimens per orientation and overhang angle.

Wall Number	Overhang Angle	Horizontal	Vertical	Diagonal
1	0°	6	6	0
2	0°	0	0	3
3	75°	4	6	0

Additionally 18 specimens were extracted from HSLA sheet material, six for each direction. This allows the comparison of the WAAM wall with the sheet material in terms of anisotropy.

The specimens were measured at three locations with a caliper gauge with an accuracy of 0.01 mm to determine the test area. For the strain measurement, marks were placed at the gauge length $5.65 \cdot \sqrt{A}$ defined by [22] for tensile specimens in relation to the test area A. For the Digital image correlation (DIC) measurement a stochastic pattern was applied on every specimen with a printed water transfer film. This was achieved by using a four-layer system, consisting of an adhesive primer, a white color primer, the printed water transfer foil and a matting final varnish. The achieved feature size of the pattern is approx. 130 µm.

2.2. Tensile Test Setup

The tensile tests were carried out at room temperature in compliance with [22]. The strain was measured with a Fielder PS-E50 laser extensometer on one side of the specimen and a two-camera Dantec Dynamics Q-400 DIC system was used to measure the displacement field on the opposite side. The testing machine used is a servo-hydraulic 250 kN MTS 318.25. The tensile load was measured with a force transducer. The tests were carried out under displacement control. The axial load, displacement and strain were recorded at a frequency of 100 Hz, while the recording frequency of the DIC system was 20 Hz. The force signal was fed to the DIC system via analog input.

The analysis of the test data was carried out in compliance with EN ISO 6892-1 (2016) [22] using MATLAB.

2.3. DIC Measurement

The two-camera DIC measurement and evaluation was performed with the Dantec Dynamics ISTRA 4D software. Schneider-Kreuznach TOURMALINE 2.8/50 C objectives were attached to the two 5 Mpixel Baumer VCXG-51M cameras. The stereo system has a working distance of 415 mm and a stereo angle of 23 °. This results in a FOV of 63.3 mm × 53.0 mm and an average image scale of 39 pixel/mm.

For the evaluation, a subset size of 19 pixel with a step size of 17 pixel was chosen. Hence resulting in an approximate subset size of 490 µm with a step size of 440 µm.

The post-evaluation analysis of the measurement data was again carried out with MATLAB. The variance errors were calculated from rigid body movement measurements of the same specimen with the identical evaluation settings. The measured coordinates have a mean variance of $2.2 \times 10^{-8}\,\mathrm{mm}^2$. The displacement fields were filtered using a LOWESS filter. The logarithmic and engineering strains were calculated from deriving the filtered displacement fields over the measured coordinates. In the following, the engineering strains are denoted by ε and the logarithmic strains by ε'.

The tensile test data and the DIC measurement were matched via the force signal. In this way, each image can be directly linked to a point in the tensile test data. A coordinate system was created for every DIC measurement with the origin at the center point of the parallel area, the x-axis parallel to the sides of the parallel area and the z-axis as the normal vector of the best fit plane of the specimen surface without load. The subset of the maximum strain at the point of the tensile strength was used to serve as the center point of a virtual strain gauge on the measurement area. This strain gauge has an original length of $5.65 \cdot \sqrt{A}$ and can therefore be used to determine the elongation at break. Furthermore, it offers the possibility to compare this strain with the strain measured via the laser extensometer in order to determine possible bending effects. The Young's modulus was calculated using the mean strain of the laser extensometer and that of the virtual strain gauge. The Poisson's ratio can be calculated directly from the strain fields:

$$\nu = -\frac{\varepsilon'_1}{\varepsilon'_2}$$

The strain fields from steps with $0.1 \cdot R_{p,0.2} \leq \sigma_n \leq 0.3 \cdot R_{p,0.2}$ were used to calculate the Possion's ratio. For each step, the strains along the virtual gauge were averaged and used for the calculation. The resulting value is the median value of all steps within the given range.

To determine the Cauchy stress, the strain measurement is used to approximate the actual area A. Since only the strains on the surface are measured, it is assumed that the strain in the thickness direction is the same as in the width direction. Therefore, the actual area can be calculated via

$$A = b \cdot t = A_0 \cdot \left(1 + {\varepsilon_y}^2\right)$$

The Cauchy stress can then be calculated by the quotient of the measured force and the actual area.

$$\sigma = \frac{F}{A} = \frac{F}{A_0 \cdot \left(1 + {\varepsilon_y}^2\right)}$$

2.4. Material Model

The Cauchy Stress and the logarithmic strain are the basis for the calculation of the material model. The finite element method software ABAQUS 2017 was used for all simulations.

For the elastic part of the material model, a linear and isotropic material model can be used, since the Young's modulus should not differ much between the specimen orientations. The command `*ELASTIC` is used with its default type `ISOTROPIC`. Input parameters are the Young's modulus E and the Poisson's ratio ν. For both parameters the median value of all tests was used.

The plastic part of the material model is a combination of the two-stage RAMBERG-OSGOOD model with a HILL yield surface. Both can be added with the `*PLASTIC` command.

The HILL yield surface allows the modeling of anisotropic yielding. It consists of 6 yield ratios which can be calculated from the yield stresses of the different material orientations:

$$R_{11} = \frac{\overline{\sigma}_{11}}{\sigma^0}, \quad R_{22} = \frac{\overline{\sigma}_{22}}{\sigma^0}, \quad R_{33} = \frac{\overline{\sigma}_{33}}{\sigma^0}, \quad R_{12} = \frac{\overline{\sigma}_{12}}{\tau^0}, \quad R_{13} = \frac{\overline{\sigma}_{13}}{\tau^0}, \quad R_{23} = \frac{\overline{\sigma}_{23}}{\tau^0}$$

$\overline{\sigma}_{ij}$ is the yield stress value of the material direction ij and σ^0 is the reference stress. The value of R_{12} can be derived from the diagonal tensile test:

$$R_{12} = \frac{1}{\left[\frac{4}{3}\left(\frac{\sigma^0}{\overline{\sigma}^{45°}}\right)^2 - \frac{1}{3}\left(\frac{1}{R_{33}}\right)^2\right]^{\frac{1}{2}}}$$

The yield ratios are given as input values of the `*POTENTIAL` option of the `*PLASTIC` command.

The two-stage RAMBERG-OSGOOD model is a description of metal plasticity. The strain is calculated with the following two equations as a function of the magnitude of the stress σ:

$$\varepsilon' = \begin{cases} \dfrac{\sigma}{E} + 0.002\left(\dfrac{\sigma}{\sigma_{0.2}}\right)^n & \text{for} \quad \sigma \leq \sigma_{0.2} \\ \dfrac{\sigma - \sigma_{0.2}}{E_{0.2}} + \left(\varepsilon'_u - \varepsilon'_{0.2} - \dfrac{\sigma_u - \sigma_{0.2}}{E_{0.2}}\right)\left(\dfrac{\sigma - \sigma_{0.2}}{\sigma_u - \sigma_{0.2}}\right)^{m_u} + \varepsilon'_u & \text{for} \quad \sigma_{0.2} < \sigma \leq \sigma_u \end{cases} \tag{1}$$

$\sigma_{0.2}$ and σ_u are the yield and ultimate stresses. $\varepsilon'_{0.2}$ and ε'_u are defined as the strains at yield and at ultimate stress. $E_{0.2}$ is the tangent modulus at the yield point and can be calculated with the following equation:

$$E_{0.2} = \frac{\sigma_{0.2}}{\frac{\sigma_{0.2}}{E} + 0.002 \cdot 1^n}$$

The exponents n and m_u can be derived via regression from the stress and strain measurements. To use this model in ABAQUS Equation (1) has to be evaluated for an array of stress values and given with the corresponding logarithmic plastic strain as input to the `*PLASTIC` command.

2.5. Simulation

The simulation is used as a benchmark test to confirm that the model shows similar mechanical behavior as the specimen. Therefore, only a linear four-sided shell element of the type `S4R` is used. It is fixed at the bottom edge in vertical direction and on one side edge for horizontal movement. On the top edge, a vertical displacement is applied as a ramp function up to an end value matching the engineering strain at tensile strength. The element has a width of 1 mm, a height of 1 mm and a shell thickness of 1 mm. The vertical reaction force `RF2` and the vertical displacement `U2` at one node on the top edge are the outputs. The nominal stress in the element can then be calculated from the reaction force divided by the element area of 1 mm^2. The engineering strain is obtained by dividing the vertical displacement by the height of the element.

3. Results

3.1. Tensile Tests

In the following part, the results of the tensile tests are presented. In Figure 3 the stress is plotted over the strain for all tests, split by the overhang angles. It is apparent that horizontal specimens have a higher yield stress than vertical and diagonal specimens for both overhang angles. The diagonal and vertical specimens have a similar stress-strain

curve and lie within the same scatter band. A direct differentiation of the linear-elastic behavior between the specimen orientations is not possible.

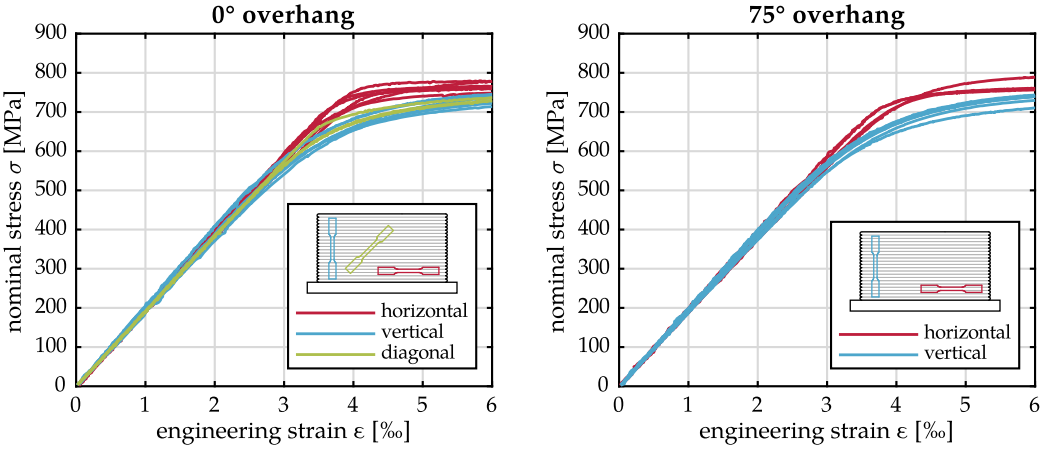

Figure 3. Stress-strain curves for specimens with different overhang angles and orientations.

The results for the mechanical parameters for an analysis in compliance with EN ISO 6892-1 (2016) [22] are listed in Table 2.

Table 2. Mechanical properties results analyzed in compliance with EN ISO 6892-1 (2016) [22].

Overhang Angle	Orientation	Specimen Number	Young's Modulus E MPa	Yield Stress $R_{p,0.2}$ MPa	Tensile Strength R_m MPa
0°	diagonal	5	197,655	734	884
0°	diagonal	6	196,009	728	885
0°	diagonal	7	197,826	723	893
0°	horizontal	1	200,342	777	903
0°	horizontal	2	199,466	748	901
0°	horizontal	3	201,964	760	887
0°	horizontal	4	202,575	765	891
0°	horizontal	5	201,114	779	897
0°	horizontal	6	199,889	763	910
0°	vertical	1	197,541	734	890
0°	vertical	2	203,562	740	893
0°	vertical	3	203,754	735	891
0°	vertical	4	195,381	726	885
0°	vertical	5	202,012	717	891
0°	vertical	6	198,242	709	895
75°	horizontal	2	198,235	756	878
75°	horizontal	4	201,962	760	896
75°	horizontal	5	198,504	759	897
75°	horizontal	6	194,393	791	911
75°	vertical	1	201,749	735	896
75°	vertical	2	202,854	738	893
75°	vertical	3	203,389	739	889
75°	vertical	4	198,909	736	891
75°	vertical	5	199,497	726	894
75°	vertical	6	199,254	706	893

The results of the mechanical properties of the tensile tests are shown in Figure 4. For each specimen orientation, a box plot shows the scatter between the minimum and maximum value with a dashed line. The colored box describes the 25 and 75% quantile values, the line inside the box represents the median value. This allows the comparison of the mechanical property results of the specimens from WAAM walls with and without overhang and from HSLA sheet material.

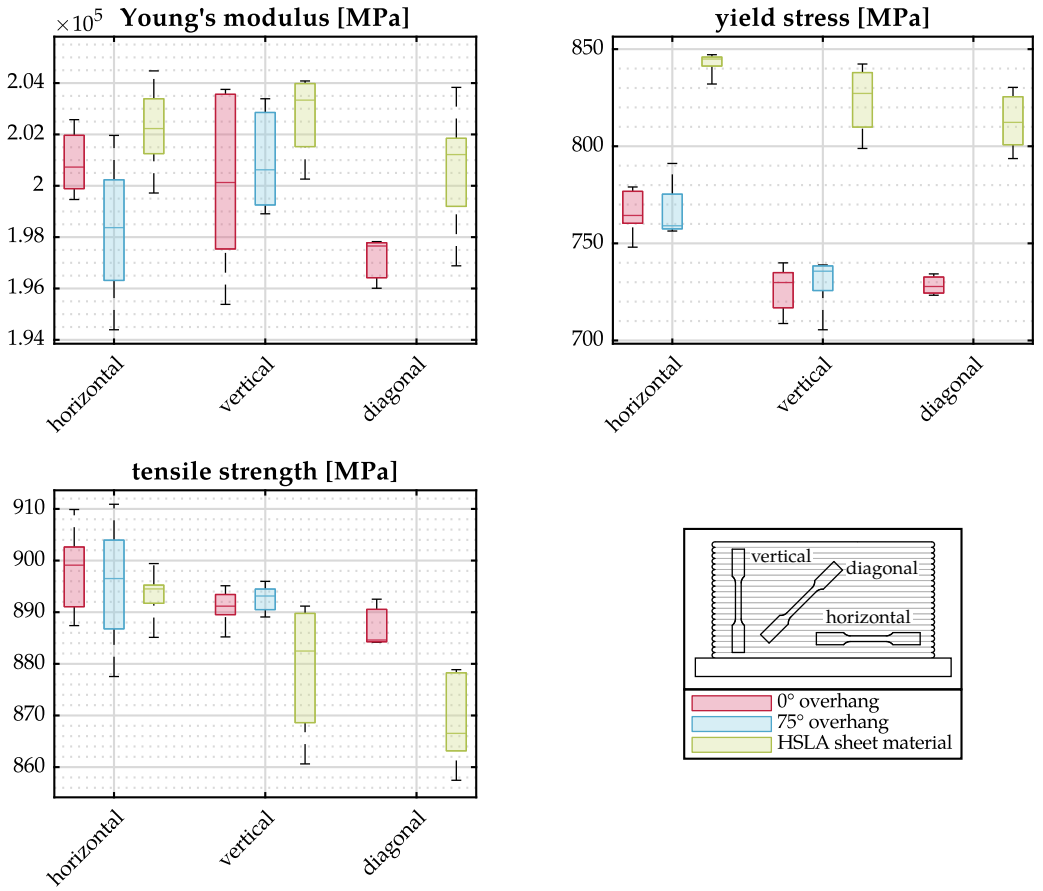

Figure 4. Young's modulus, yield stress and tensile strength box plots for different specimen orientations.

Compared to HSLA sheet material, the Young's modulus results for the specimens from WAAM walls have a higher scatter. The median Young's modulus is also smaller for all WAAM specimens. The orientation of the specimen in the WAAM walls and the overhang angle both show no clear effect on the Young's modulus results of the specimens.

The results of the yield stress for the different orientations of WAAM specimens differ by approximately 4.5% between the horizontal and the vertical specimens. The results of the specimens made of sheet material show less dependence on the orientation than those of the WAAM wall specimens. Similar to the Young's modulus results, the influence of the overhang angle is negligible.

The orientation of the specimen has no clear effect on the tensile strength of the specimens extracted from WAAM walls. The results for the different overhang angle are almost identical. The specimens from sheet material show a larger anisotropy of the tensile strength than the specimens from WAAM walls.

3.2. DIC Measurement

In Figure 5, the engineering strain fields at 0.2% proof stress are shown for different orientations from walls without overhang. In the diagonal specimen, the layer orientation can be seen directly in the strain field. In particular, one layer exhibits a larger strain than the surrounding ones.

The vertical specimen shows the most homogeneous strain field of the three directions, while the horizontal strain field displays a large strain concentration on the right side and a strain valley on the left side of the measurement area. The layer is not directly visible in neither the vertical nor the horizontal specimen.

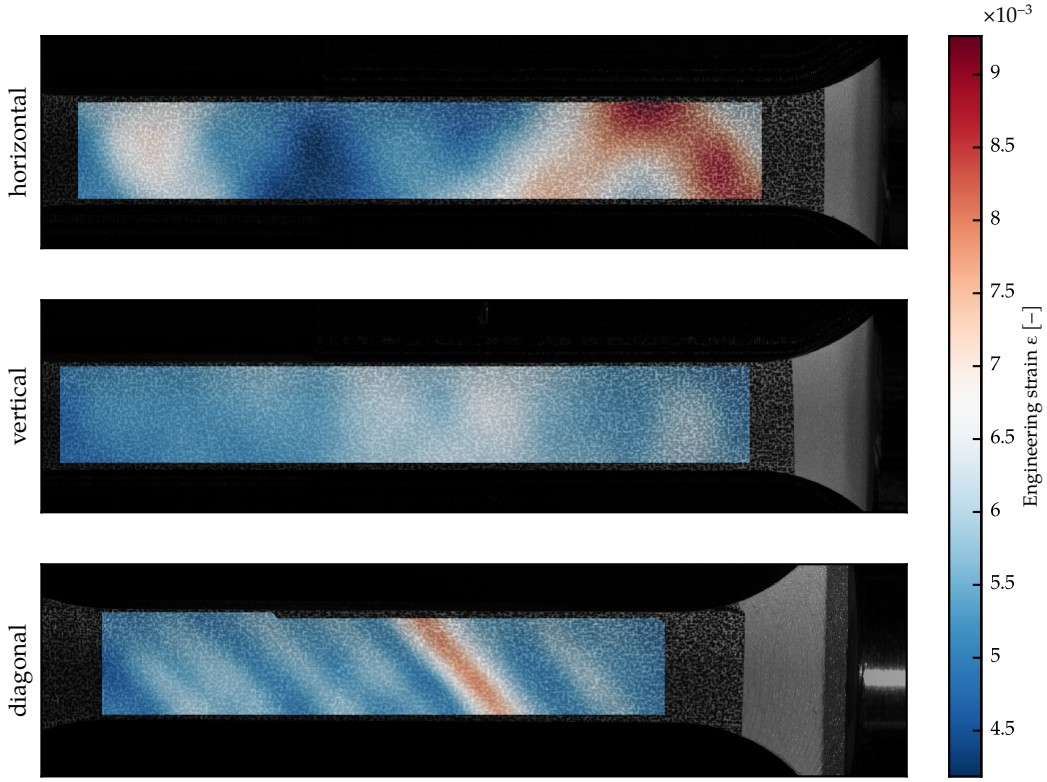

Figure 5. Engineering strain fields at 0.2% proof stress for specimens of different orientation from walls without overhang.

The Poisson's ratio and elongation at break results calculated from the DIC measurements are plotted in Figure 6 for different specimen orientations.

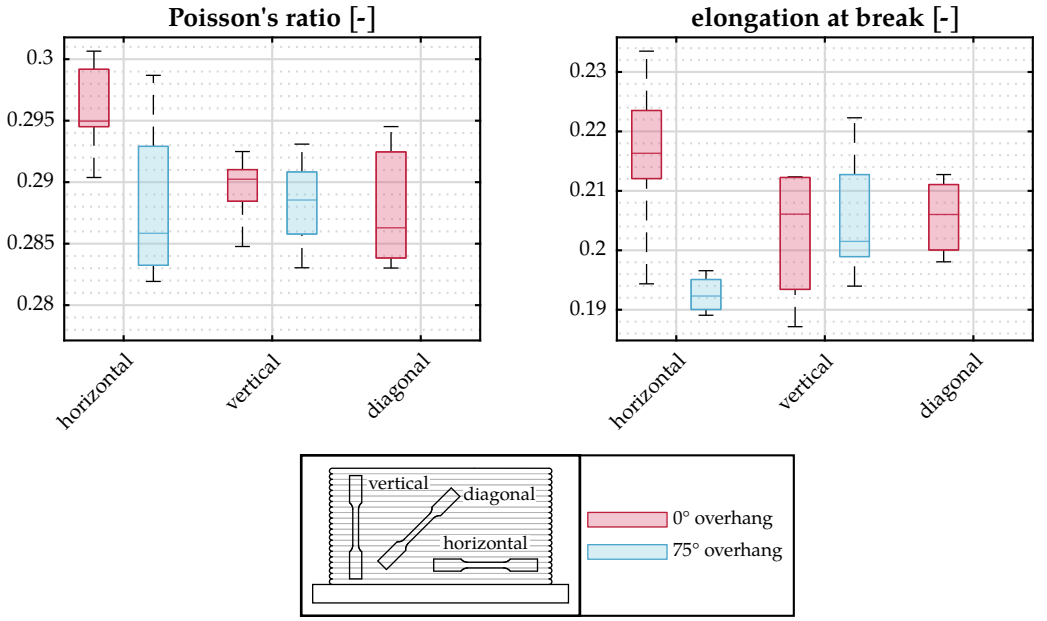

Figure 6. Poisson's ratio and elongation at break box plots for different specimen orientations.

The Poisson's ratio results for specimens without overhang show no dependence on the specimen orientation. The results for specimens of the wall with an overhang angle of 75° show a smaller median Poisson's ratio for vertical specimens. The difference, although noticeable, is small in absolute value.

The elongation at break ranges between 19% and 23% for all specimens. An influence of the specimen orientation is not clearly visible due to the scatter of the results.

3.3. Material Model

The results of the tensile tests show that the anisotropy of HSLA WAAM walls is relatively small. Only the results for the yield stress show a significant difference for specimens of different orientations. The overhang angle has no clear effect on the material properties of the tensile specimens. Therefore, the same material model can be used for 0 and 75° walls.

The modeling and analysis steps described in Section 2.4 result in the material model parameters listed in Table 3 for HSLA WAAM walls. A differentiation between the overhang angles was not considered necessary due to the small differences in the results of the material properties as shown in the previous sections.

Table 3. Material model parameters.

E MPa	ν -	R_{11} -	R_{22} -	R_{33} -	R_{12} -	R_{13} -	R_{23} -	$\sigma_{0.2}$ MPa	n -	σ_u MPa	ε'_u -	m_u -
202,100	0.29102	1.0	0.9506	1.0	0.9400	1.0	1.0	767.4	36.264	999.8	0.1009	1.2563

In Figures 7–9 the benchmark results for the different material orientations are shown with the nominal stress plotted over the engineering strain. For comparison with the test result, they also contain the scatter band of all measured stress-strain curves for specimens of the respective direction. The left plot shows the first 10% of engineering strain and the full stress range. For a detailed view of the yield point the range between 0 and 2% is extracted and plotted in the right subplot of the respective figure.

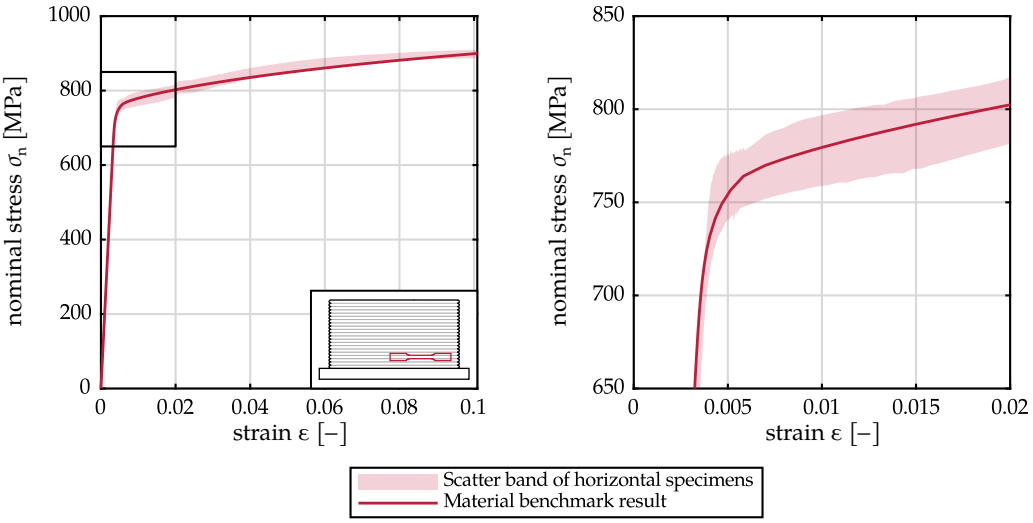

Figure 7. Material benchmark result and scatter band of all tests for a horizontal specimen.

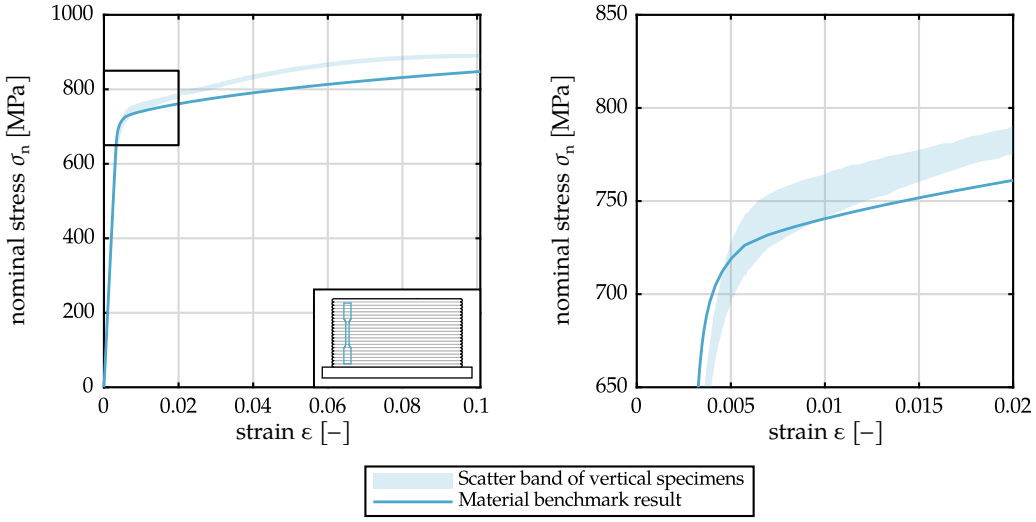

Figure 8. Material benchmark result and scatter band of all tests for a vertical specimen.

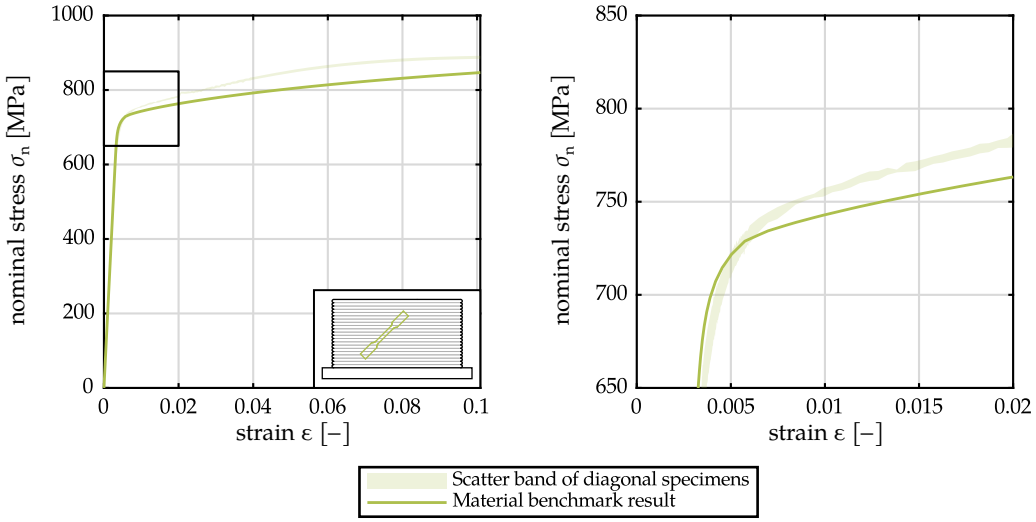

Figure 9. Material benchmark result and scatter band of all tests for a diagonal specimen.

As can be seen, the model accurately describes the horizontal behavior since it was calibrated on data of this direction (view Figure 7). The material model response coincides with the middle of the scatter band of all horizontal specimens. The vertical and diagonal response of the material model differs from the measured material behavior. While the onset of plasticity matches with the measured data, the stress response of the model after yielding is smaller than observed in the experiment (see Figures 8 and 9). For the vertical specimens, the onset of yielding also does not match with the material behavior of the vertical specimens: The material model curve lies above the scatter band for strains smaller than the strain at 0.2% proof stress. The same result can be seen for the diagonal response of the material model.

4. Discussion

The results of the tensile tests show that the overhang angle exerts no visible influence on the mechanical properties of the tensile specimens. The orientation of the specimens, on the other hand, has an influence on the yield stress: for horizontal specimens, the median yield stress is approximately 4.5% higher than for vertical and diagonal specimens. For the other material specimens, no direct influence of the orientation can be derived from the results. Similar results have been found by [12]: the yield strength shows only a minor dependence on the specimen orientation. For Young's modulus, tensile strength

and elongation at break, the specimen orientation has no significant influence. A clear anisotropy cannot be detected. However, for [20] the yield strength and elongation at break depend on the build-up direction. Only the tensile strength seems to be independent. [19] only finds an anisotropic elongation at break.

The tensile specimens made of HSLA sheet material also show anisotropy of the yield stress, but to a lesser extend. The material behavior is similar to that of HSLA WAAM walls.

Compared to [12], the diagonal specimens show strain concentrations corresponding to the layer orientation. For other orientations of the specimens, no strain concentrations were observed with respect to the layer orientation.

Based on the experimental results, a material model was developed. The resulting model, based on isotropic hardening with a RAMBERG-OSGOOD model and a HILL yield surface, is able to reproduce anisotropic yielding but underestimates the stresses after yielding in the vertical and diagonal directions. Thus, the tensile strength in vertical and diagonal orientation is underestimated. This can result in larger deformations when using this material model. A comparison to a similar material modeling technique of [10] is limited, as the material behavior of stainless steel and HSLA steel is in generally different.

Overall, this work demonstrates that the material behavior of WAAM HSLA steel is similar to that of HSLA sheet material and can be characterized as nearly isotropic regarding the main material properties. The developed advanced material model can reflect this anisotropy. For a conclusive assessment of the material behavior with regard to construction industry, further investigations on as-built specimens and WAAM components are required. This is important for the structural design of WAAM components and for future certification concepts.

5. Conclusions

Based on reliable process parameters, extensive experimental and numerical investigations are carried out to characterize the influence of layer orientation (0°, 45°, 90°) and overhang angle (0°, 75°) on the mechanical parameters of WAAM high-strength low-alloy steel (HSLA) walls. The results have been compared to HSLA steel sheet material with regard to civil engineering applications:

- It is shown that comparable characteristics for Young's modulus, yield stress and tensile strength exist.
- The influence of the loading direction at the material level is generally similar to that of HSLA steel sheet material. However the sheet material in this study shows a greater anisotropy than the WAAM walls.
- The yield stress shows a slight dependence on the layer orientation for WAAM walls.
- The influence of the layer orientation on Poisson's ratio and the elongation at break is not clearly visible.
- The overhang angle does not influence the material parameters.

The research highlights the importance of extensive experimental investigations for the development of advanced numerical models. In the future, this material model still needs be validated in tests on complex "as-built" WAAM components, such as tubes or K-nodes, with loads in the plastic range.

Author Contributions: Conceptualization, H.J. and J.U.; methodology, H.J. and J.U.; software, H.J.; validation, H.J.; formal analysis, H.J.; investigation, H.J.; resources, J.M., J.H. and K.T.; data curation, H.J.; writing—original draft preparation, H.J. and J.U.; writing—review and editing, H.J., J.U., J.M., J.H. and K.T.; visualization, H.J.; supervision, J.U., J.H. and K.T.; project administration, J.U., J.H. and K.T.; funding acquisition, J.U., J.H. and K.T. All authors have read and agreed to the published version of the manuscript.

Funding: The research presented in this paper is being conducted within the project "Wire Arc Additive Manufacturing (WAAM) of Complex and Refined Steel Components (A07)." The project is part of the collaborative research center "Additive Manufacturing in Construction—The Challenge of Large Scale," funded by the Deutsche Forschungsgemeinschaft (DFG, German Research Foundation)—

project number 414265976—TRR 277. We acknowledge support by the Open Access Publication Funds of the Technische Universität Braunschweig.

Data Availability Statement: The raw/processed data required to reproduce these findings cannot be shared at this time as the data also forms part of an ongoing study.

Conflicts of Interest: The authors declare no conflict of interest.

Abbreviations

The following abbreviations are used in this manuscript:

DED	Direct energy deposition
DED-EB	Direct energy deposition with electron beam
DIC	Digital image correlation
HSLA	High-strength, low-alloy steel
GMAW	Gas metal arc welding
GPAW	Gas plasma arc welding
GTAW	Gas tungsten arc welding
WAAM	Wire and arc additive manufacturing

References

1. Kuhlmann, U.; Dürr, A.; Bove, S.; Roth, J.; Knecht, W. DASt-Richtlinie für geschweißte K- und KK-Knoten aus Rundhohlprofilen unter Ermüdungsbeanspruchung—Kommentar. In *Stahlbau-Kalender 2021*; Kuhlmann, U., Ed.; Wiley Online Library, Wilhelm Ernst & Sohn: Berlin, Germany, 2021; pp. 329–365.
2. Kyvelou, P.; Buchanan, C.; Gardner, L. Numerical simulation and evaluation of the world's first metal additively manufactured bridge. *Structures* **2022**, *42*, 405–416. [CrossRef]
3. MX3D. Connector for Takenaka. Available online: https://mx3d.com/industries/construction/connector-for-takenaka/ (accessed on 10 January 2023).
4. Feldmann, M.; Kühne, R.; Citarelli, S.; Reisgen, U.; Sharma, R.; Oster, L. 3D–Drucken im Stahlbau mit dem automatisierten Wire Arc Additive Manufacturing. *Stahlbau* **2019**, *88*, 203–213. [CrossRef]
5. Lange, J.; Feucht, T.; Erven, M. 3D printing with steel. *Steel Constr.* **2020**, *13*, 144–153. [CrossRef]
6. Reimann, J.; Henckell, P.; Ali, Y.; Hammer, S.; Rauch, A.; Hildebrand, J.; Bergmann, J.P. Production of Topology-optimised Structural Nodes Using Arc-based, Additive Manufacturing with GMAW Welding Process. *J. Civ. Eng. Constr.* **2021**, *10*, 101–107. [CrossRef]
7. Relativity Space. Relativityspace Rocket Fuel Tank. Available online: https://www.relativityspace.com/ (accessed on 1 January 2023).
8. Haden, C.V.; Zeng, G.; Carter, F.M.; Ruhl, C.; Krick, B.A.; Harlow, D.G. Wire and arc additive manufactured steel: Tensile and wear properties. *Addit. Manuf.* **2017**, *16*, 115–123. [CrossRef]
9. Kyvelou, P.; Slack, H.; Daskalaki Mountanou, D.; Wadee, M.A.; Britton, T.B.; Buchanan, C.; Gardner, L. Mechanical and microstructural testing of wire and arc additively manufactured sheet material. *Mater. Des.* **2020**, *192*, 108675. [CrossRef]
10. Hadjipantelis, N.; Weber, B.; Buchanan, C.; Gardner, L. Description of anisotropic material response of wire and arc additively manufactured thin-walled stainless steel elements. *Thin-Walled Struct.* **2022**, *171*, 108634. [CrossRef]
11. Xin, H.; Tarus, I.; Cheng, L.; Veljkovic, M.; Persem, N.; Lorich, L. Experiments and numerical simulation of wire and arc additive manufactured steel materials. *Structures* **2021**, *34*, 1393–1402. [CrossRef]
12. Huang, C.; Kyvelou, P.; Zhang, R.; Ben Britton, T.; Gardner, L. Mechanical testing and microstructural analysis of wire arc additively manufactured steels. *Mater. Des.* **2022**, *216*, 110544. [CrossRef]
13. Müller, J.; Grabowski, M.; Müller, C.; Hensel, J.; Unglaub, J.; Thiele, K.; Kloft, H.; Dilger, K. Design and Parameter Identification of Wire and Arc Additively Manufactured (WAAM) Steel Bars for Use in Construction. *Metals* **2019**, *9*, 725. [CrossRef]
14. Müller, J.; Hensel, J.; Dilger, K. Mechanical properties of wire and arc additively manufactured high-strength steel structures. *Weld. World* **2022**, *66*, 395–407. [CrossRef]
15. Rodrigues, T.A.; Duarte, V.; Avila, J.A.; Santos, T.G.; Miranda, R.M.; Oliveira, J.P. Wire and arc additive manufacturing of HSLA steel: Effect of thermal cycles on microstructure and mechanical properties. *Addit. Manuf.* **2019**, *27*, 440–450. [CrossRef]
16. Sun, L.; Jiang, F.; Huang, R.; Yuan, D.; Guo, C.; Wang, J. Anisotropic mechanical properties and deformation behavior of low-carbon high-strength steel component fabricated by wire and arc additive manufacturing. *Mater. Sci. Eng. A* **2020**, *787*, 139514. [CrossRef]
17. Lin, Z.; Goulas, C.; Ya, W.; Hermans, M.J. Microstructure and Mechanical Properties of Medium Carbon Steel Deposits Obtained via Wire and Arc Additive Manufacturing Using Metal-Cored Wire. *Metals* **2019**, *9*, 673. [CrossRef]
18. Ermakova, A.; Mehmanparast, A.; Ganguly, S.; Razavi, J.; Berto, F. Investigation of mechanical and fracture properties of wire and arc additively manufactured low carbon steel components. *Theor. Appl. Fract. Mech.* **2020**, *109*, 102685. [CrossRef]

19. Yildiz, A.S.; Davut, K.; Koc, B.; Yilmaz, O. Wire arc additive manufacturing of high-strength low alloy steels: Study of process parameters and their influence on the bead geometry and mechanical characteristics. *Int. J. Adv. Manuf. Technol.* **2020**, *108*, 3391–3404. [CrossRef]
20. Hu, M.J.; Ji, L.K.; Chi, Q.; Ma, Q.R. Microstructures and Fatigue Properties of High-Strength Low-Alloy Steel Prepared through Submerged-Arc Additive Manufacturing. *Materials* **2022**, *15*, 8610. [CrossRef] [PubMed]
21. Gardner, L.; Kyvelou, P.; Herbert, G.; Buchanan, C. Testing and initial verification of the world's first metal 3D printed bridge. *J. Constr. Steel Res.* **2020**, *172*, 106233. [CrossRef]
22. *ISO 6892-1:2016*; Metallic Materials—Tensile Testing—Part 1: Method of Test at Room Temperature. ISO: Geneva, Switzerland, 2016.

Disclaimer/Publisher's Note: The statements, opinions and data contained in all publications are solely those of the individual author(s) and contributor(s) and not of MDPI and/or the editor(s). MDPI and/or the editor(s) disclaim responsibility for any injury to people or property resulting from any ideas, methods, instructions or products referred to in the content.